

OPTICAL APPLICATIONS OF URANIUM THIN-FILM COMPOUNDS
FOR THE EXTREME ULTRAVIOLET AND SOFT X-RAY REGION

by

Richard Lunt Sandberg

Submitted to the Department of Physics and Astronomy in partial fulfillment
of graduation requirements requirements for the degree of
Bachelor of Science

Brigham Young University

August 2004

Advisor: David D. Allred

Thesis Coordinator: Justin Peatross

Signature: _____

Signature: _____

Department Chair: Scott D. Sommerfeldt

Signature: _____

Abstract

I report the measured reflectances from Beamline 6.3.2 at the Advanced Light Source (ALS) at Lawrence Berkeley National Laboratory (LBNL) of air-oxidized sputtered uranium, reactively sputtered (O_2) uranium oxide, and reactively sputtered (N_2) uranium nitride thin films. These are compared with measurements of the reflectance of nickel, gold, and iridium thin films (commonly used soft x-ray reflectors for astronomy and synchrotrons) from 2.7 to 11.6 nm at 5° , 10° , and 15° grazing incidence. These show that uranium, as UO_2 , can fulfill its promise as the highest known single surface reflector for this portion of the soft x-ray region, being nearly twice as reflective as nickel in the 5-10 nm region. (Its reflectance at 10° also exceeds that of Au, Ni, and Ir for most of this range.) There are important discrepancies between UO_2 's and UN's actual reflectance with those predicted by the previously reported optical properties of these uranium compounds. There is a need to determine the actual constants. Uranium-based optics will find application in many types of optical devices such as zone plate mirrors, thin film reflectors, and filters.

Acknowledgments

I had outstanding help from a number of people in the Physics & Astronomy and Chemistry Department at BYU. I want to thank Hollilyn Drury and Megan Rowberry for aiding in sputtering the air-oxidized uranium films studied. An SPIE scholarship and a BYU ORCA Scholarship and BYU Department of Physics and Astronomy research funds made this research possible for me. Also, I acknowledge gratefully the financial contributions of V. Dean and Alice J. Allred and Marathon Oil Company (US Steel) for gifts to Brigham Young University for thin-film research. Thanks to all the members of the BYU EUV team for their support, especially Kristi Adamson, Jiang Guilin, and Amy Baker for XPS, Jed Johnson and Luke Bissell for sputtering films and aiding with ALS measurements, Nikki Farnsworth, Mindy Tonks for AFM, and Winston Larsen for TEM and AFM. I thank Dr. Ritva Keski-Kuha for providing the sputtered iridium samples. Eric Gullikson and Andy Aquila at ALS Beamline 6.3.2 at LBNL have provided tremendous aid in data interpretation, reduction, and analysis. I especially want to thank my sweet wife Deanne for all of her sacrifice in supporting me in my research efforts and for caring for our daughter Karadyn.

List of Figures	v
List of Tables	v
1 Introduction	1
1.1 Why Uranium?	2
1.2 Applications	4
1.3 Project Focus	6
2 Thin Film Preparation and Characterization	8
2.1 Sample Preparation	8
2.1.1 Sputtering	8
2.1.2 Evaporation	11
2.2 Characterization	13
2.2.1 X-ray Diffraction	13
2.2.2 X-ray Photoelectron Spectroscopy	17
2.2.3 Atomic Force Microscopy	23
2.2.4 Transmissin Electron Microscopy	27
2.3 ALS Reflectance Measurements	29
3 Reflectance Comparison, Analysis, and Applications	32
3.1 Reflectance Comparison	32
3.2 Comparison to Calculated Reflectance	35
3.3 Applications for Uranium Thin Tilms	39
4 Conclusion	42
References	43

List of Figures

1	The $d - \beta$ plot for uranium and several other elements at 4.48 nm	3
2	The computed reflectance at 5° from grazing for Ni, NiO, U, and UO ₂	4
3	Sputtering chamber cross-section	9
4	Fitting for thickness of NiO on Ni with IMD	14
5	XRD scan of UO 18 sample	15
6	XRD scan of gold sample	15
7	XRD scan of nickel sample	16
8	Surface scan of UO18 samples with major XPS lines annotated	18
9	XPS Depth Profiling of U018 Sample	19
10	U4f _{5/2} and U4f _{7/2} peaks of UO18 sample	20
11	O1s peak of UO18 sample	21
12	XPS surface scan of NiO with major XPS lines annotated	22
13	Schematic of an AFM tip in contact with a sample surface	23
14	Low and high frequency roughness compared	24
15	Affects of 1.0 nm RMS roughness on thick uranium layer	25
16	Power Spectral Density of surface roughness on UO 18	26
17	Diffraction pattern of a uranium oxide sample produced by TEM	27
18	Schematic of beamline 6.3.2 at the ALS	29
19	Measured reflectance of UO _x from ALS beamline 6.3.2 at 5°	30
20	Measured reflectance of UO ₂ , UN, NiO on Ni, Ir, and Au at 5°	33
21	Measured reflectance of UO ₂ , UN, NiO on Ni, Ir, and Au at 10°	34
22	Measured reflectance of UO ₂ , UN, NiO on Ni, Ir, and Au at 15°	35

23	Reflectance comparison of measured and calculated uranium oxide	36
24	XANES data taken at the ALS of uranium oxide and thorium oxide	38

List of Tables

1	Important XPS Lines	18
2	RMS Roughness of UO18 Sample	26
3	First Order Efficiency for 100 nm Thick	

Chapter 1

Introduction

Recently, the extreme ultraviolet (EUV) and soft x-ray region of the electromagnetic spectrum (between about 1 and 100 nm or 20 eV to 5 keV) has become increasingly important in technological applications. The next generation of optical technologies will include EUV astronomy, high resolution soft x-ray microscopy for medical/materials science imaging, and EUV computer lithography. These technologies all require optical devices: mirrors, lenses, and other imaging equipment. The Brigham Young University's EUV Optics research team has been studying the properties of uranium as an EUV optical material for several years. Here I review my research conducted at Brigham Young University (BYU) which has been to find and implement applications for uranium-based optics for the EUV and soft x-ray region. I have been able to publish several articles on this research in conjunction with presentations at scientific conferences. Much of this thesis comes from those articles which shall be noted in the references [1-3]. Also, this research is a follow-up on the research on uranium oxide that was begun by Shannon Lunt, a former Master's Student at BYU. Her thesis is referred to frequently [4]. Also, I aided Marie Urry of BYU in studying the uranium nitride samples she prepared. These results can also be found in her thesis [5]. Here I use her results to compare the reflectance of UN to those I prepared and studied.

1.1 Why Uranium?

Uranium has promising optical properties for application as an optical device over much of the EUV and soft x-ray portions of the spectrum [1-8]. Uranium metal is very dense (bulk density about 19 g/cm³). It has 92 electrons that may interact with photons over many energy ranges. One of the unique properties of uranium is that over a range of about 6 nm (200 eV) it has a very large index of refraction coupled with very modest absorption. Materials with low absorption and high index of refraction have desirable properties for EUV applications, such as zone plates and multilayer mirrors. The index of refraction of materials in the EUV does not vary much from unity, so the common convention is to express the complex index of refraction (\tilde{n}) as follows:

$$\tilde{n} = n + ik = 1 - \mathbf{d} + i\mathbf{b} . \quad (1)$$

Equation 1.1 gives the following relations for index of refraction (n) and absorption (k)

$$n = 1 - \mathbf{d} \quad (2)$$

$$k = \mathbf{b} . \quad (3)$$

The $d - \beta$ scatter plot (Fig. 1) for various elements at 4.47 nm (277 eV) shows that no other element has a d as high, and its β is remarkably low. The reported beta of uranium is less than one-quarter of Ni and other 3d elements and less than one-sixth the value of Ir and other 5d elements. The question has been, in light of uranium metal's susceptibility to oxidation, whether its promise can be realized. Here we will see that it can.

current widely used materials for EUV and soft x-ray optics. Fig. 2 shows the reflectance calculated from the CXRO website.

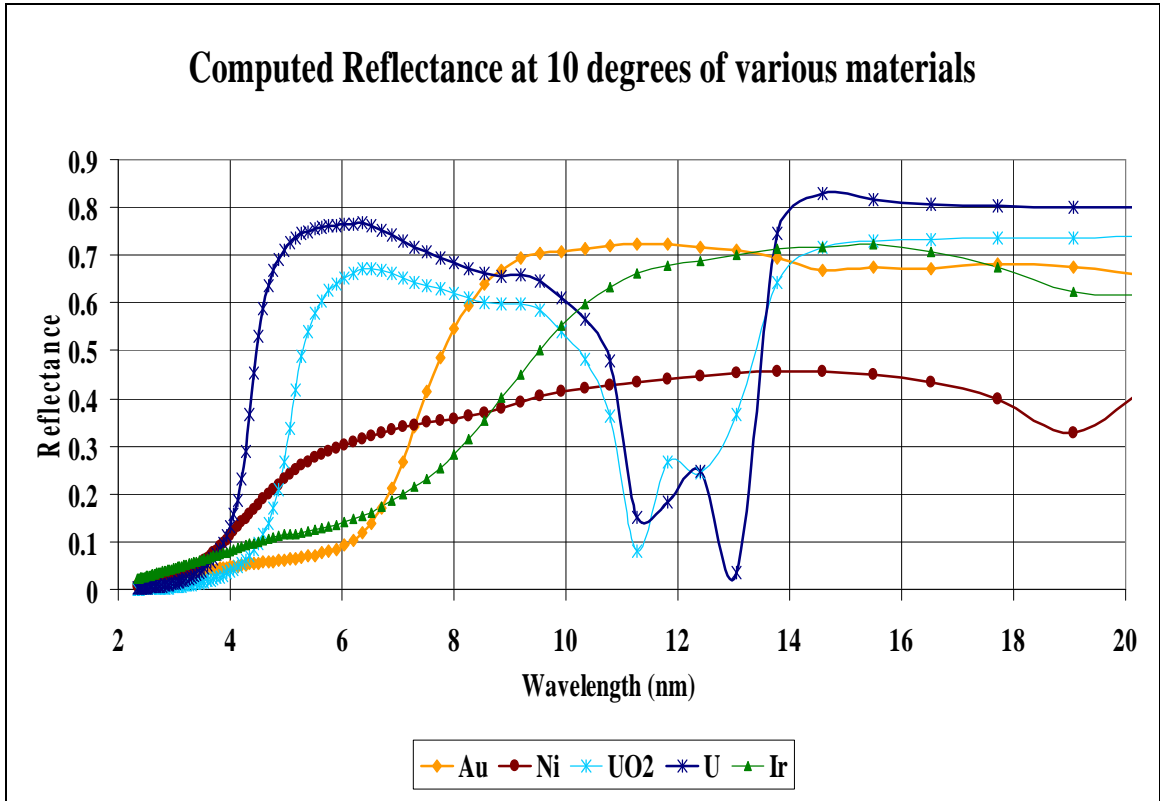


Fig. 2: The reflectance at 10° from grazing for Ni, NiO, U, and UO2 calculated from the CXRO website [9].

1.2 Applications

There have been several efforts to use uranium and, later, its oxides, as constituents in reflectors.

1. A group at MOXTEK, Inc. of Orem, Utah prepared and measured U/Sc multilayer mirrors in the water window in 1993-5. This approach relies on the low absorption of uranium to allow many layers in a multilayer to participate in

multilayer reflectivity and uses the high delta to produce high amplitude reflectance at each interface [14].

2. The BYU EUV group used uranium in the late 1990's to prepare several near-normal-incidence U/Si mirrors with high reflectance (23%) at 30.2 nm (41 eV) and low reflectance (~1%) at 59.0 nm (21 eV) for the IMAGE spacecraft which currently orbits the Earth [6]. It should be noted that the design incorporated the fact that the top uranium layer is oxidized. This was our first realization that the native oxide which forms on uranium might be useful in its own right in optics.
3. A third potential application of uranium for broadband, low-angle-of-incidence mirrors for the 4.1 to 12.4 nm (100 to 300 eV) range was suggest to us by Prof. Webster Cash (University of Colorado) [15]. He had performed calculations in the mid 1990s indicating that uranium might produce high reflectance single-surface mirrors for x-ray astronomy. The first reported soft x-ray measurements of uranium films with and without an ultra thin carbon "barrier" top layer appear in [7].

As seen above, uranium has a high predicted reflectance from the reported optical properties due to its high density and large number of electrons. However, uranium is chemically active and will quickly oxidize in ambient air. Uranium nitride has the highest uranium atom density of known compounds according to data in Cordfunke [16].

Additionally, Black et al [17] stated that uranium nitride is resistant to bulk oxidation.

Urry showed that uranium nitride thin films sputtered at room temperature exhibit some surface oxidation [5].

Other potential applications for the uranium as a highly reflective coating in this wavelength region include astronomical applications, soft x-ray microscopy which would improve the resolution of visible light microscopy by more than one-hundred times, and EUV lithography for computer chip manufacturing. Soft x-ray microscopy and EUV lithography are especially exciting applications due to their numerous technological applications. Soft x-ray microscopy has extremely valuable applications in medical and biological imaging and material science research as described in Attwood and Takemoto [18,19]. According to the National Technological Roadmap for Semiconductors, EUV lithography will be the industry standard for computer chip manufacturing by the end of the decade [19].

1.3 Project Focus

In this thesis, I will discuss uranium compounds as thin film reflectors (mirrors) and single layer zone plate lenses. We will see how uranium can increase the low-angle reflectance currently available for thin-film single-layer reflectors at about 140-250 eV (5-9 nm) [1-3,6,7]. In the following chapters, I will discuss how the samples analyzed were prepared and studied. Also, we will see recent reflectance measurements from 100-460 eV (2.7 to 11.6 nm) comparing uranium as naturally oxidized uranium (UO_2), uranium nitride (UN), nickel (and nickel oxide), iridium, and gold single layer reflectors. As mentioned earlier, nickel, iridium, and gold were chosen for the reflectance comparison because of their wide use as a thin-film reflective coating in optical systems for the EUV and soft x-ray range [6]. The samples' reflectances were measured at the Advanced Light Source's Beamline 6.3.2 at the Lawrence Berkley National Laboratory.

The low-angle reflectance of uranium oxide and uranium nitride surfaces exceeds that of traditional coatings over a large wavelength range. Furthermore, I will compare the reflectance measurements from these samples with reflectances predicted by existing optical constants for uranium.

Chapter 2

Thin Film Preparation and Characterization

2.1 Sample Preparation

All of the samples except the iridium sample were prepared here at BYU. The uranium-containing samples were deposited by magnetron sputtering, UN via RF sputtering in one system and the two kinds of uranium oxide (air oxidized uranium and reactive sputtered UO_x) via DC sputtering in another [4,5]. The nickel and gold were deposited by thermal evaporation in a third system. All the BYU systems were cryopumped. The base pressure for all samples was about 3×10^{-6} torr.

The iridium samples were sputtered at the Goddard Space Flight Center on glass slides [20]. The other materials were deposited on a variety of substrates including the following: pieces of standard polished, silicon-test wafers (100 orientation), fused quartz slides, and carbon coated TEM (transmission electron microscope) grids. All samples were deposited at room temperature. The deposited films ranged from 10 to 50 nm in thickness. The surface roughness (rms) of several silicon wafers was measured via atomic force microscopy (AFM) to be ~ 0.2 nm over a 100 by 100 nm area [7].

2.1.1 Uranium compounds deposited through sputtering

All the uranium-based samples were sputtered in one of two stainless steel chambers from a uranium target (Manufacturing Sciences, Oak Ridge, TN) in independently controlled flowing argon, and if needed, reactive gases with a pressure

range of 1 to 15×10^{-3} torr. The uranium sputter targets used here were of depleted uranium metal (less than 0.2% U-235). Dr. David Allred calculated the decay per second of depleted uranium as about 0.238 alphas, twice as many betas and miscellaneous L x rays for each cm^2 of a 10 nm film at bulk density [7]. The users' solid angle of detection of these will be considerably less than 2π steradians. (Half go down into the substrate and are absorbed.) So counts from the mirror will be small compared to background for soft x-ray applications.

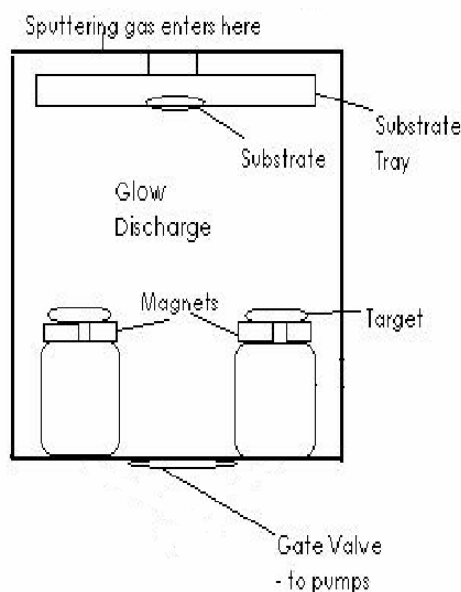


Fig. 3: “Davy” sputtering chamber cross-section [4].

Two processes were used for depositing uranium oxide as described in previous works by the BYU EUV group. Both processes involved sputtering in a stainless steel vacuum chamber named Davy (see Fig. 3). One process was to sputter a uranium thin film and let it oxidize in air. A 20 nm film is thoroughly oxidized in a day (TEM and x-ray photoelectron spectroscopy, or XPS, show oxidized uranium to be mostly UO_2) [8]. Lunt

reactively sputtered uranium in an oxygen partial pressure of 3×10^{-4} torr [4]. More details are found in Lunt [4] and Oliphant [8]. The uranium oxide sample (named UO 18) was deposited on April 10, 2003, and was sputtered at an argon partial pressure of 2.88×10^{-3} torr in the system named Davy.

The uranium mononitride sample (named UN04) was deposited on September 30, 2003 at an argon partial pressure of 1×10^{-3} torr and a nitrogen partial pressure of 1×10^{-5} torr in the second system named Joey. The residual gas composition in the system Joey after bake-out was of nitrogen, oxygen and argon at the ratios found in air as determined by a Ferran Scientific millipole analyzer (MPA). A small turbo pump was used in parallel with the Cryotorr 8 pump to remove hydrogen and helium which are not pumped well by the cryopump. The pumping system was throttled by mostly closing the gate valve in front of the cryopump prior to sputtering. We employed a 20-sccm full-scale mass flow controller to set the Ar pressure to the level needed to ignite the plasma. For the UN samples, nitrogen was flowed through a separate line to the chamber and was controlled by a low-flow, sapphire diaphragm valve immediately above the chamber. More details of how the UN samples were prepared can be found in Urry [5]. During sputtering the MPA was used to set the nitrogen flow to achieve the desired nitrogen partial pressure of 1×10^{-5} torr. A quartz crystal thickness monitor in front of the shutter allowed us to set the sputter rate to the desired amount, usually about 0.1 to 0.4 nm/sec.

The target thickness for the uranium oxide sample after oxidation was about 30 nm as measured by x-ray diffraction (XRD). (A uranium film oxidizing completely to UO_2 is calculated, based on handbook densities, to approximately double in thickness, so the initial films were thinner [21].) The XRD data will be shown later. After sputtering,

the uranium was allowed to oxidize naturally in laboratory air since its removal from the vacuum chamber 63 days before measuring thickness. Prior to this study, studies of the oxidation rates of uranium thin films have been conducted [8]. Uranium is subject to extensive oxidation in laboratory air, about 6 nm in 13 min, and more than 13 nm in a day. Oliphant further showed that the uranium oxidizes into films of UO_{2+x} ($x \sim 0$) which can be a few nanometers thick under typical laboratory conditions (room ambient).

It should be noted that many bulk oxides of uranium are known. Even for a given composition, such as UO_3 , many different crystal structures are known. Also UO_2 tolerates a large range of nonstoichiometry. The value of x in UO_{2+x} can reach 0.25 before inducing crystal changes. Members of our group have recently studied these subtleties using XPS and TEM [22,23].

Here, I will denote the uranium oxide as UO_x or UO_2 because it is closest to UO_2 . For the uranium oxide, the UO_2 stoichiometry and handbook density of 10.59 g/cm^3 will be used in calculation in accordance with Oliphant's findings [8]. When I refer to the reflectance and other properties of the uranium oxide film used in the study, it should be understood that this means the most abundant natural oxide of uranium, UO_2 .

2.1.2 Ni and Au deposition through thermal evaporation

The nickel and gold films were prepared by evaporating Ni wire from a resistively heated tungsten boat (RD Mathis Co.) in a large, cryopumped, stainless steel "bell jar" coater. The base pressure of the system was $3.2 \times 10^{-4} \text{ Pa}$ ($2.4 \times 10^{-6} \text{ torr}$). A quartz crystal monitor was used to measure the evaporation rate. The source was shuttered as the voltage to the tungsten boat was increased. When the evaporation rate reached about 1-2

nm/s, the shutter was opened and the substrates were coated. Fast deposition rates are known to be preferable in obtaining the highest reflectance for aluminum and many materials. This is probably due to their limiting the extent to which impurities, usually oxygen, are drawn into the film from residual air and water vapor in the vacuum. After the monitor recorded about 91 nm of film the voltage to the source was cut, the box was vented to air and the films removed for further study. They were allowed to naturally oxidize for two days before XRD thickness measurement and up to several weeks before measurement at the Advanced Light Source.

At the time the first films were deposited, the tooling factor of the crystal monitor for the position of the substrates was not known. After the thickness of the film on Si was determined via XRD (see below) to be about 50 nm the tooling factor of the crystal monitor was seen to be about 55%. The crystal monitor was set significantly closer to the evaporation boat than the substrates, though to one side. So this tooling factor is consistent with geometry. Since the surface roughness of polycrystalline materials usually increases with increasing film thickness and surface roughness decreases reflectance, thinner Ni films were desirable. Calculations had indicated that all Ni films thicker than about 30 nm should have the same low-angle, soft x-ray reflectance over our range of interest. The target thickness for the nickel film was chosen as between 30 and 60 nm.

Before evaporating the gold sample, a small amount of chromium was evaporated onto the substrate to aide in the adhesion of the gold layer on top. Once again, calculations showed that a gold layer of 30 nm was desirable. The two samples deposited on silicon test wafers are referred to as NiO-on-Ni and Au deposited.

2.2 Characterization

2.2.1 Thickness determination: Characterization with XRD and IMD Fitting.

Thin-film interference of x rays was used to determine the thickness of the deposited thin films. Using a Scintag[®] X-ray diffractometer (XRD), we measured the low-angle reflectance maxima and minima. The Scintag diffractometer produces collimated x ray radiation from a rotating copper target, which was scattered off of the sample. A liquid nitrogen cooled intrinsic germanium detector in photon counting mode was gated to accept K_{α} radiation (0.154 nm) and reject K_{β} and bremsstrahlung radiation above and below $Cu K_{\alpha}$. Angle scans at low angles (usually from 1-3.5°, 2 θ , grazing incidence angles) were taken. These scans showed interference fringes. At first-order approximation, the data can be modeled with an equation which resembles the Bragg diffraction,

$$m\lambda = 2d\sin\theta \quad (4)$$

where m is the diffraction order, λ is the wavelength of the diffractometer radiation in the material being measured, d is the layer thickness, and θ is the angle between the incident and refracted beam. The Bragg equation as written above does not take into account the refraction of the x rays in the material because the index of refraction for all elements in the EUV does not vary significantly from unity. It is adequate for approximating the thickness of the film but to properly obtain the thickness we must match the spectra with a computer model. We used IMD (an optical properties modeling and curve-fitting

program) to model our layers [24]. Then by adjusting the thickness of the modeled layer, the diffraction peaks of the model and the measured XRD scan can be compared until the numbers of peaks in the same angle interval are the same and the peak positions match (see Fig. 4). There are several disadvantages to using this technique, including that we do not account for interdiffusion of layers, composition gradients, or surface roughness.

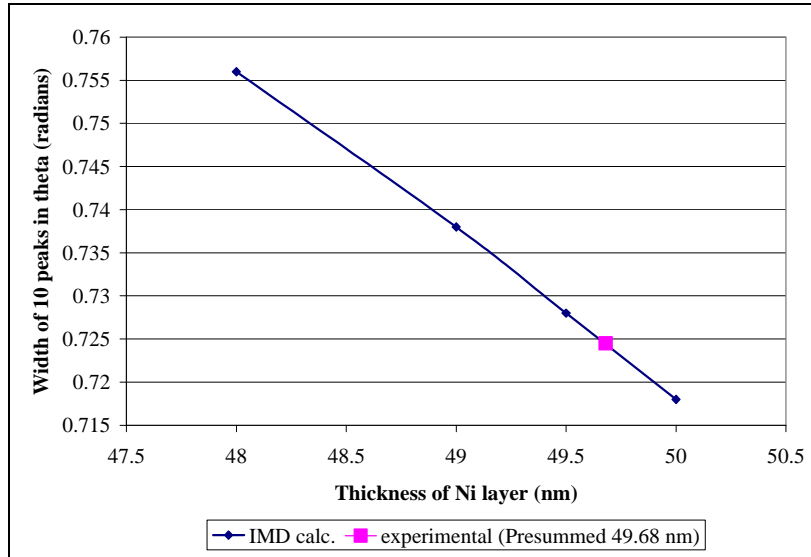


Fig. 4: Fitting for thickness of NiO on Ni by adjusting the thickness in an IMD model of the sample. The change in angle for 10 diffraction peaks from IMD changes with thickness until it agrees with 10 peaks from XRD measurement.

Figs. 5-7 are the XRD plots of the three samples studied here (UO 18, gold, and nickel). The XRD plots for UN are found in Urry's thesis [5].

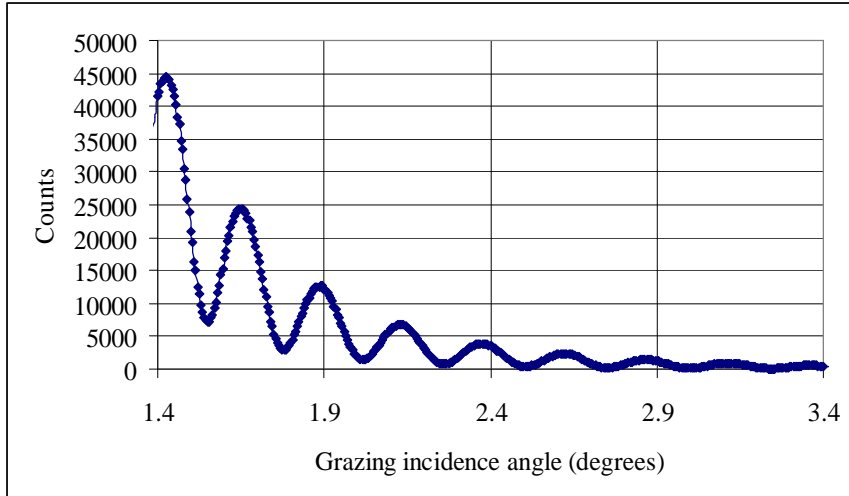


Fig. 5: XRD scan of UO 18 sample (theta-theta scan).

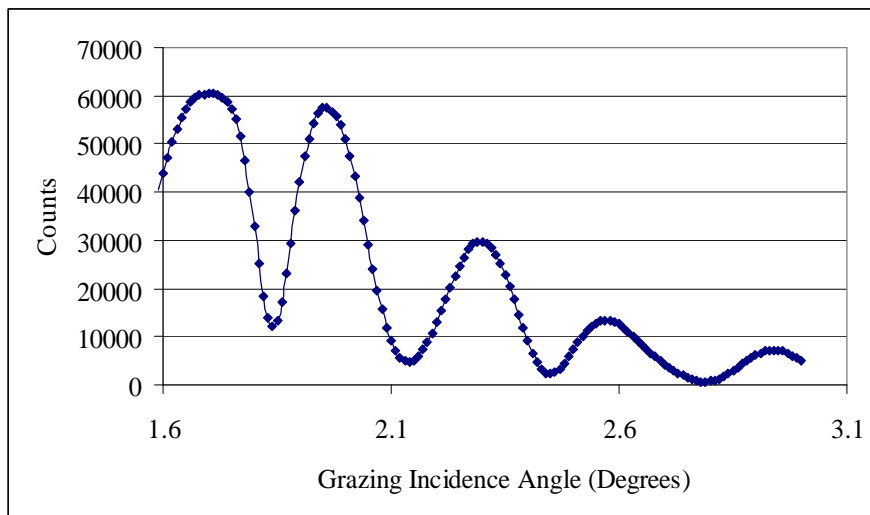


Fig. 6: XRD scan of gold sample (theta-theta scan).

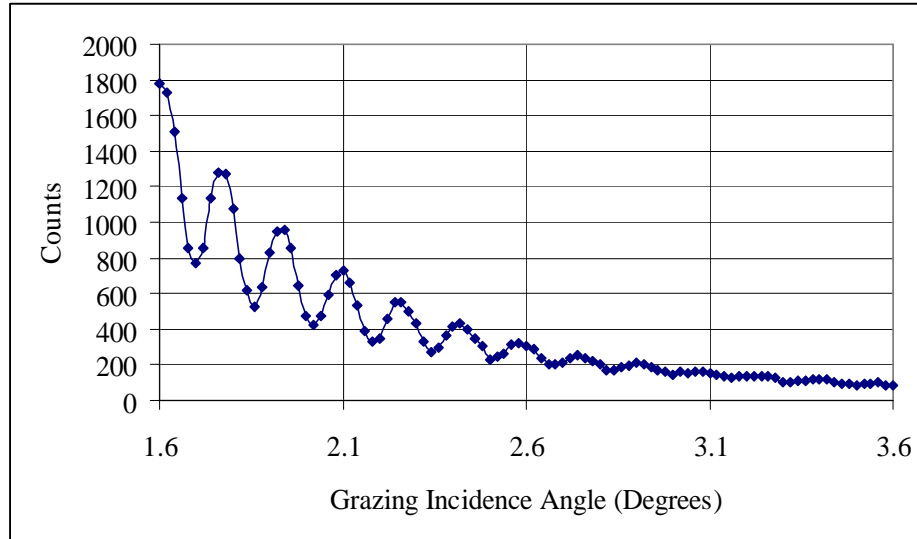


Fig. 7: XRD scan of nickel sample (theta-theta scan).

The computed value for thickness is then approximately the same as the real layer thickness. For nickel, this thickness was 49.7 nm. For gold, this thickness was 29.5 nm. For the uranium oxide sample this thickness was 31.8 nm. For uranium nitride this thickness was 38 nm. These approximations do not take into account composition gradients between layers nor surface roughness. As stated earlier, efforts to develop an algorithm that takes these into account are underway in the BYU EUV group. The iridium samples were measured at the Advanced Light Source (ALS) at Lawrence Berkeley National Laboratory (LBNL), but were lost in the return trip and therefore could not be measured by XRD.

The transmission of the nickel film on quartz and the ellipsometric constants for the nickel film on silicon were also measured using a John A. Woollam Company M2000D model spectroscopic ellipsometer with rotating compensator for the interval 189 to 1000 nm. The transmission and the ellipsometric data were concatenated and modeled using the WVASE32 version 3.347 software that comes standard with the instrument. At

~50 nm the Ni film was still sufficiently transparent in the visible range to constrain the thickness of the nickel as finite. Fixing the thickness to that given by XRD gave a mean square error (MSE) of 3.78. The indices of NiO were not known, but the model could still constrain the thickness of the native oxide which forms on our Ni films in a period of a few days to less than 2 nm and probably greater than 1 nm.

2.2.2 X-Ray Photoelectric Spectroscopy

To determine the composition of our samples, we used x-ray photoelectric spectroscopy (XPS). The calibration of the system is done about the carbon 1s peak at a binding energy of 285 eV once a month using a gold target. Further details on the calibration and measurement procedures are found in Lunt [4] and Adamson [22]. The XPS device is also fitted with a sputter gun so that depth profiling of samples may be conducted. However, the sputter rates vary from sample to sample, and therefore cannot be absolutely determined. The uranium oxide samples and the nickel sample were studied in September, 2003, several months after the deposition of the nickel sample and about 18 months after the deposition of the uranium oxide samples. The XPS results of the uranium nitride samples are found in Urry [5].

The XPS device exposes the samples by either aluminum (1487.7 eV) or magnesium (1253.6 eV) K_{α} x-rays and the kinetic energy of ejected electrons is measured. Photoelectrons are ejected from the surface after absorbing the incident photon or through Auger processes. From the kinetic energy of the ejected electron, we can infer its binding energy (f) from the

$$f = \hbar \mathbf{l}_i - E_k \quad (5)$$

where $h\nu_i$ is the energy of the incident x-ray and E_k is the kinetic energy of the electron.

From the binding energies, the composition of the surface can be determined and from the relative size of the count peaks, the relative abundance of elements can be determined. Table 1 summarizes several important peaks in our study.

Ni		U		Other	
Energy	Line	Energy	Line	Energy	Line
66 eV	3p3/2	100eV	5d5/2	280eV	C 1s
68 eV	3p1/2	380eV	4f7/2	398eV	N 1s
111eV	3s	390eV	4f5/2	530eV	O 1s
853eV	2p3/2	740eV	4d5/2		
870eV	2p1/2	780eV	4d3/2		
1009eV	2s				

Table 1: Important XPS lines

Surface scans of the uranium oxide samples showed that they were mostly uranium and oxygen as shown in Fig. 8.

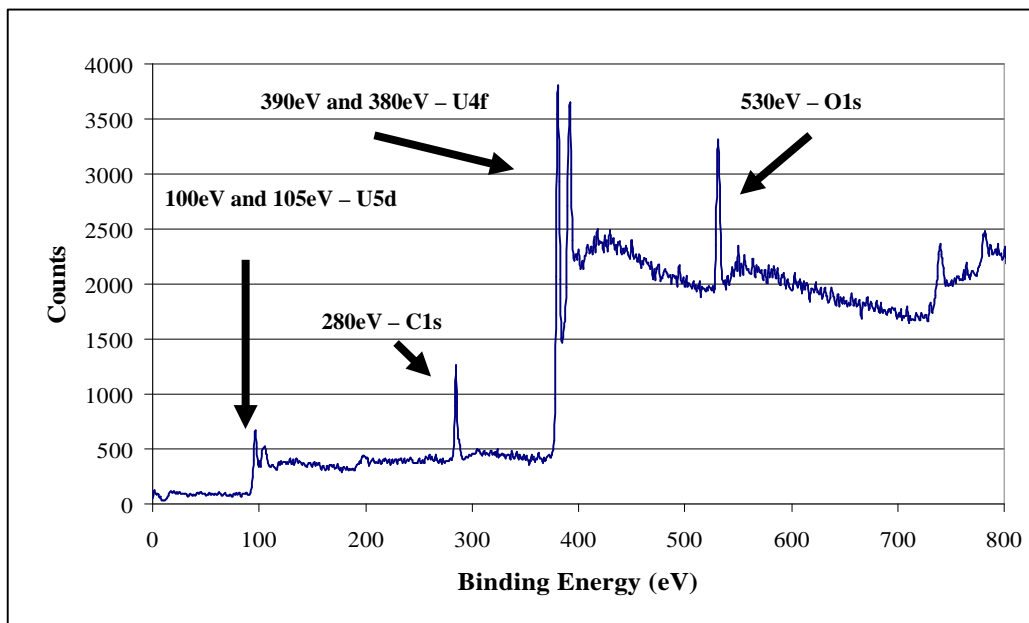


Fig. 8: Surface scan of UO18 samples with major XPS lines annotated.

For the depth profiling, sputtering times were at intervals of 3 minutes between which XPS scans were taken. The depth profiling scan shows that the relative composition of uranium is about 40% and about 60% oxygen, close to UO_2 . For more details about uranium peak position and relative composition analysis see Adamson [22]. Fig. 9 shows the relative composition of uranium and oxygen as a function of sputtering time.

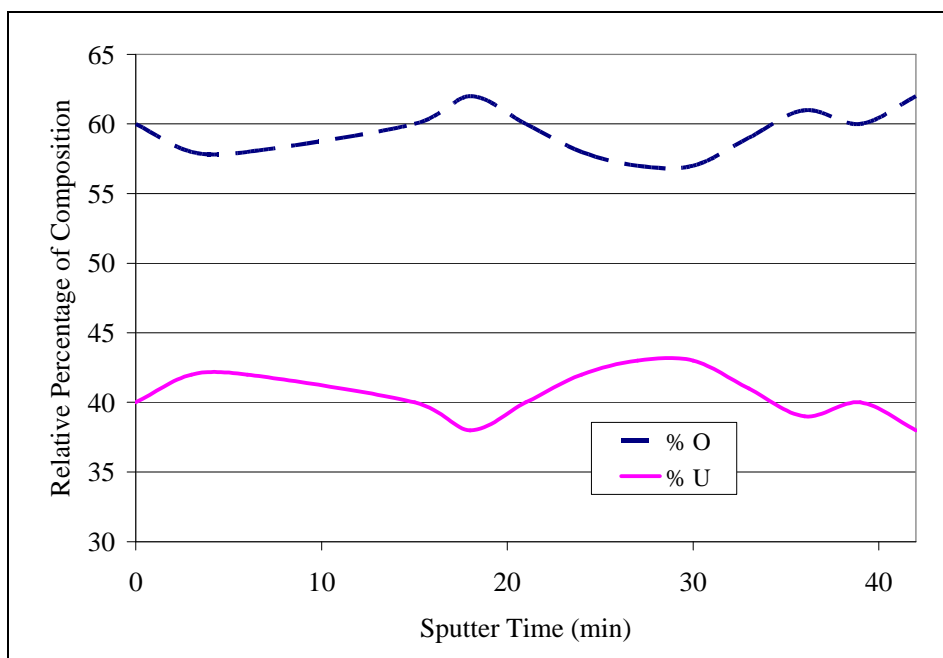


Fig. 9: XPS Depth Profiling of U018 Sample (Comparison of uranium to oxygen).

As described in Adamson [22], stoichiometry of our uranium samples can be determined from the position of the uranium and oxygen peaks. This is accomplished by comparing our peak positions to published data, specifically the extensive XPS scans of various oxidation states of uranium performed by Teretin [25]. The peak positions shift as the oxidation increases. For further details, consult Adamson [22].

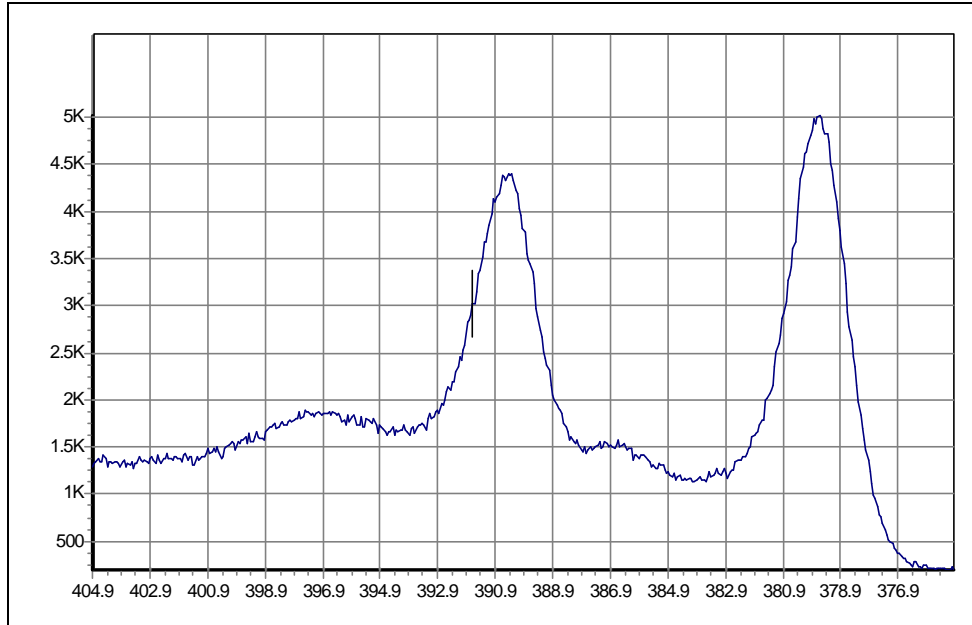


Fig. 10: U4f5/2 and U4f7/2 peaks of UO18 sample.

Fig. 10 shows the UO18 XPS scan of the uranium 4f5/2 and 4f7/2 peaks. In comparing to the data in Teretin [25], we see that the peak positions and shapes most closely resemble the $\text{UO}_2(\text{M})$ or $\text{UO}_{2.06}$ oxidation states. Notice the peak positions at 389.9 eV and 379.9 eV respectively, compared to Teretin's 392 eV and 381 eV respectively. Adamson also noticed this shift to lower energies and discussed it in [22]. Furthermore, we notice the appearance of the two smaller peaks approximately 7 eV above each of the dominant peak, corresponding to the lower oxidation states reported by Teretin.

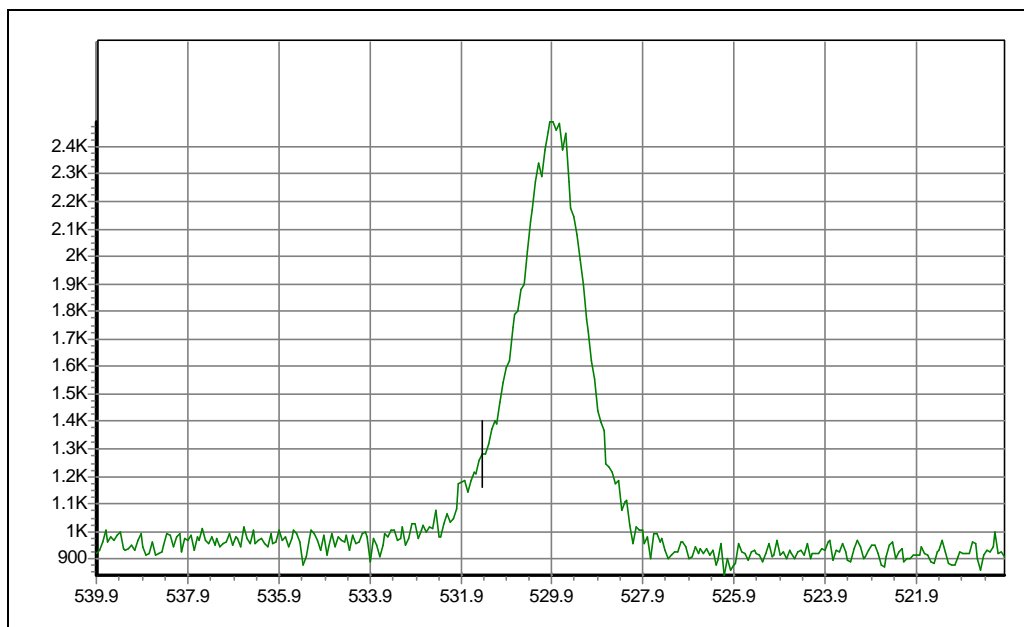


Fig. 11: O1s peak of UO18 sample

In addition to the uranium 4f peak analysis, the oxygen 1s peak can tell us the oxidation state of our samples. In fact, Teretin shows that the oxygen peak is perhaps the best indicator of uranium oxidation state as it undergoes more dramatic shape change and energy shift to higher energies. As shown in Fig. 11, the O1s peak is centered at about 529.9 eV, which is on the lower end of expected binding energies reported by Teretin, indicating our sample is mostly UO_2 . Additionally, the oxygen peak stays in relatively the same location during the duration of the depth profiling. It only shifts by 0.2 or 0.3 eV towards higher energy, leading us to believe that our composition remains fairly constant throughout the sample.

XPS scans were also conducted of the NiO sample to determine the depth of the oxidation. The NiO sample was cleaned with UV Excimer lamp which produces ozone

and intense UV light in an attempt to remove the carbon contamination on the surface. For more information on carbon contamination, consult [26,27]. The ozone quickly oxidized the surface for 3 minutes before taking data at the ALS in June, 2003. The surface was visible oxidized, so the XPS scans were conducted to determine its new composition.

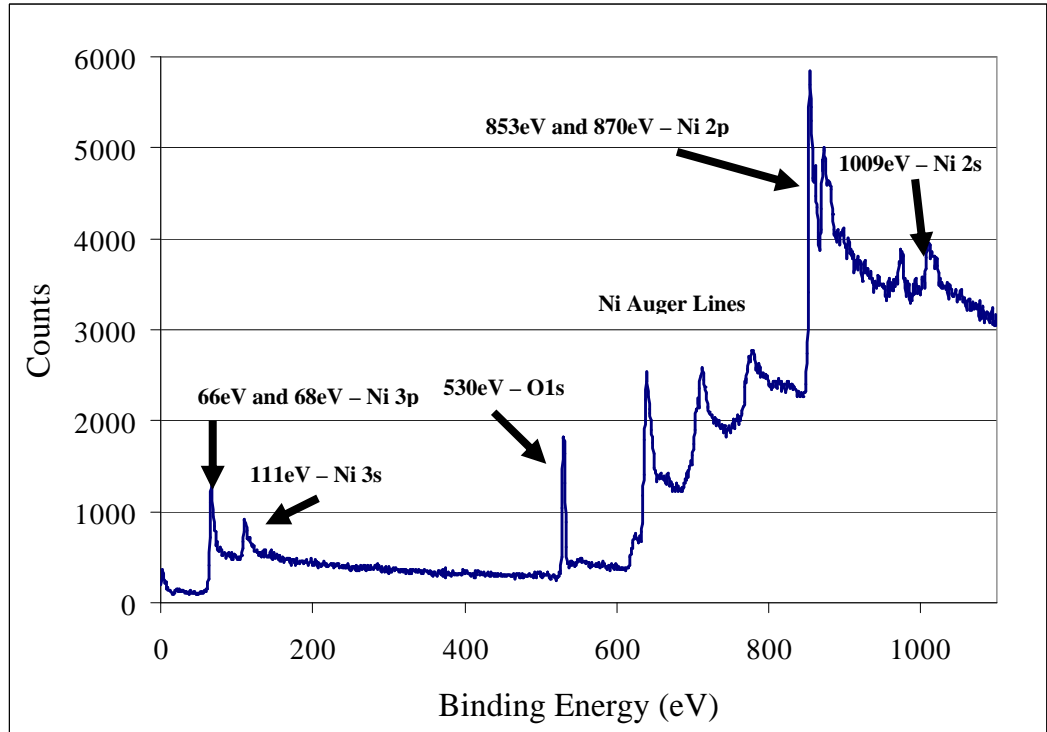


Fig. 12: XPS surface scan of NiO with major XPS lines annotated.

Later ALS reflectance comparisons to newly deposited nickel films of the relative same thickness showed that the NiO sample had a higher EUV reflectance than the non-oxidized nickel over much of the EUV range. The surface scan showed the presence of nickel and oxygen (consult Table 1 for line energies) as seen in Fig. 12.

2.2.3 Atomic Force Microscopy

Atomic force microscopy (AFM) was used to measure the surface roughness of the thin films. AFM measurements were made in tapping mode at BYU. The AFM consists of a microscopic tip on the end of a tiny cantilever that is tapped at high frequency on the surface of the samples. A laser is reflected off of the back of the tip so that as the tip goes up and down as it passes bumps and valleys in the sample, the laser light is deflected and the relative surface height can be measured (Fig. 13). The deflection of the laser is measured using a photodiode detector.

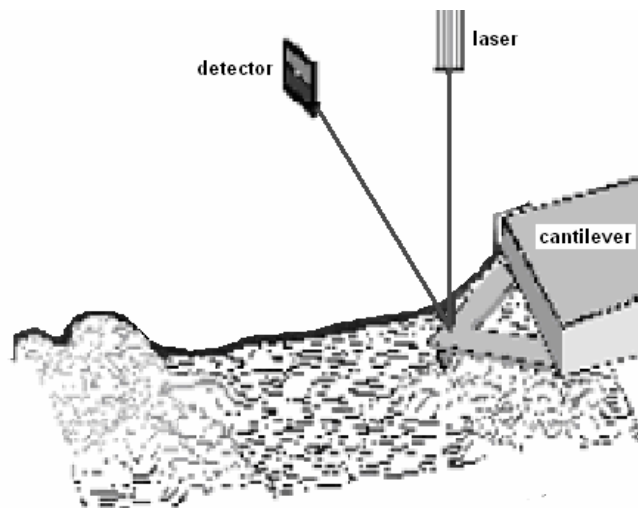


Fig. 13: Schematic of an AFM tip in contact with a sample surface [28].

The AFM measurements are important because surface roughness lowers the reflectance of thin films and complicates the calculation of optical constants. Large scale, or low frequency roughness, results in beam scattering. Diffraction effects accompany small scale, or high frequency roughness [29]. These factors arise from the imperfect nature of both the substrate and the deposition techniques.

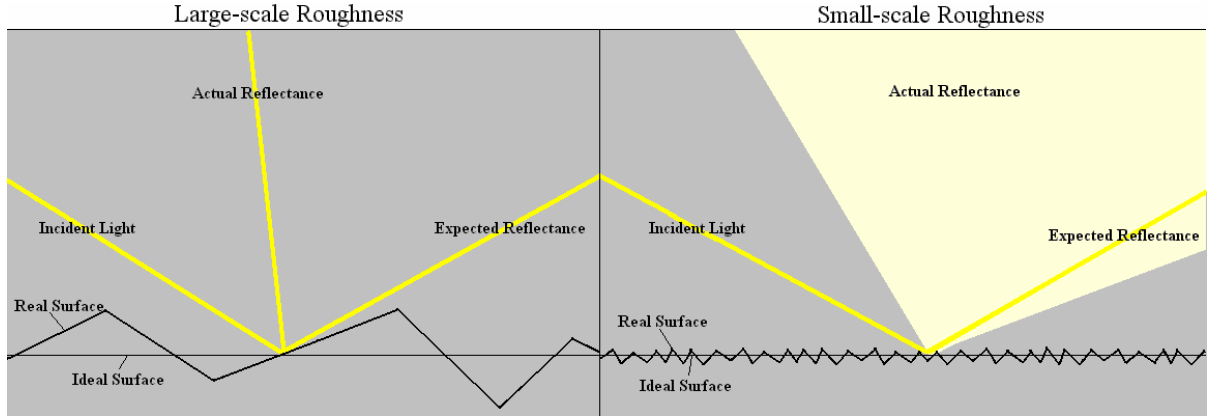


Fig. 14: Low and high frequency roughness compared [29].

Fig. 14 demonstrates how different length scales of roughness effect reflectance. Several methods attempt to model the effect of roughness. The Debye-Waller method is given by [30]:

$$R_s = R_0 e^{-\frac{4ps}{\lambda}} \quad (6)$$

where R_s is the measured reflectance, R_0 is the calculated reflectance, λ is the wavelength, and s = RMS deviation of surface. This model tends to underestimate the effects of roughness. The Nevot-Croce method is an alternative to Debye-Waller which overestimates the effects. It is represented by [31]:

$$R_s = R_0 e^{-q_1 q_2 s^2} \quad (7)$$

where

$$q_x = \frac{4pn \sin(\theta)}{\lambda} \quad (8)$$

In these two formulas, n is the real part of complex index of refraction, θ the incident angle from grazing, and s = RMS deviation of surface.

The two models can be averaged to estimate the reduction in reflectance due to roughness. Fig. 15 shows the calculated effect of roughness on reflectance from the CXRO webpage [9]. The calculated curve shows the reflectance of a completely smooth optically thick uranium oxide film at 10 nm. Notice the drop in reflectance as an effect produced by 1.0 nm RMS roughness.

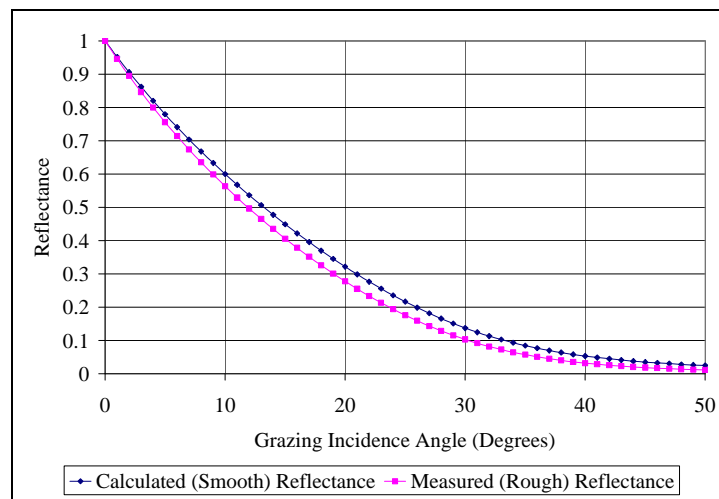


Fig. 15: Calculated effect of 1.0 nm RMS roughness on the reflectance of an optically thick uranium layer at a wavelength of 10 nm.

We took measurements at six different locations on the uranium oxide sample (named UO18 #3) over different length scales. Root mean square (RMS) roughness was measured over the length scales of 10 by 10 microns, 1 by 1 micron, and 100 by 100 nm. There is a limit in the AFM resolution due to the size of the tapping tip which is 10 nm in diameter. This limits our resolution to a length scale of about 50 nm. So, the minimum roughness scan we could perform was 100 by 100 nm.

Here are the RMS roughness values at the three length scales (Table 2).

Location	10x10 microns	1x1 micron	100x100 nm
1	1.085	1.431	1.562
2	5.458	4.031	1.774
3	7.827	0.835	0.910
4	3.799	1.340	1.290
5	2.531	0.242	0.147
6	1.791	0.202	0.170
Average	3.749	1.347	0.976
Std. Dev.	2.529	1.415	0.696

Table 2: RMS Roughness of Sample UO 18

By taking a Fourier analysis of the different length scale components of the surface roughness, we can produce the power spectral density of our samples. Fig. 16 displays the power spectral density of the surface roughness of sample UO 18.

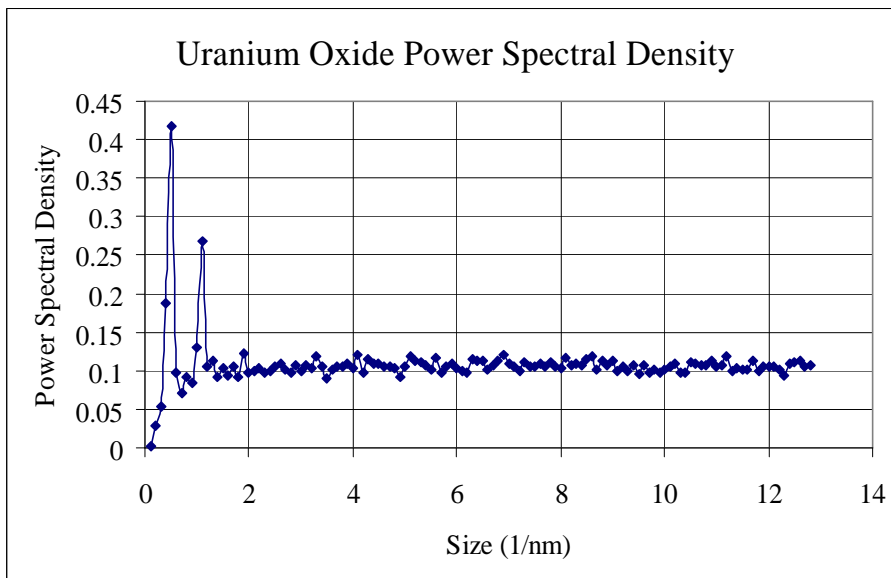


Fig. 16: Power spectral density of surface roughness on UO 18.

2.2.4 Transmission Electron Microscopy

The transmission electron microscope (TEM) is the tool that was used to obtain crystal lattice parameter for our uranium samples. Samples were prepared by depositing thin films on carbon coated TEM grids at the same time the other samples were sputtered. These TEM grid samples were then viewed in plan view. Our samples are polycrystalline in structure, so when I say that we are determining the lattice parameter, we are actually determining the average lattice parameter of an ensemble of nanocrystals. An electron beam passes down the apparatus and is focused using electrostatic lenses. Many of the electrons pass through the target and diffract. The electrons are further focused using electrostatic lenses and then hit a phosphorescent screen. This shows up as an image and can be photographed. Diffraction patterns were gathered at 200 keV or 160 keV and at a camera length of 130 cm or 110 cm, respectively. Fig. 17 shows a diffraction pattern of the UO₂ sample.

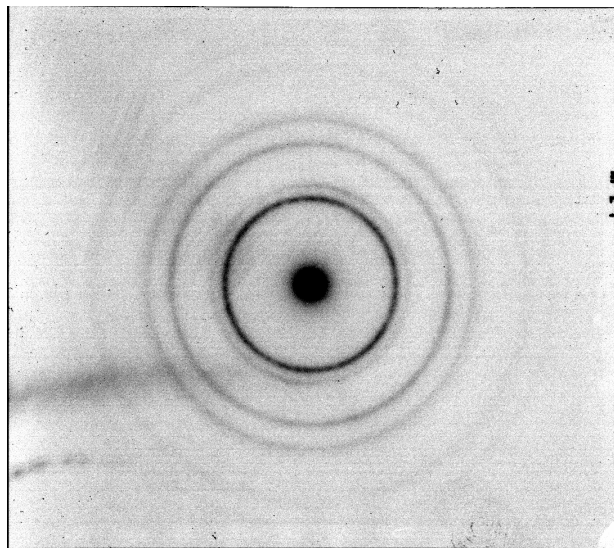


Fig. 17: Plan view diffraction pattern of a uranium oxide sample produced by TEM at a camera length of 130 cm. The darkest ring has a radius of 1.5 cm.

Once diffraction patterns were obtained, they were used to find lattice parameters. The composition of the thin films can be determined from the lattice parameters. The lattice parameter is the distance between corresponding lattice points in the crystal lattice. To find the lattice parameter the equation

$$a = \sqrt{Md} \quad (9)$$

was used, where a is the lattice spacing, M is the square of the corresponding Miller Index, and d is the distance between reflecting planes.

The interplane spacing (d) is found using an approximation of Bragg's Law, namely

$$d = \lambda \frac{L}{R}, \quad (10)$$

where λ is the de Broglie wavelength for the accelerated electrons in the beam, L is the camera length, and R is the distance from the center spot to a given ring or dot in the diffraction pattern.

Once the lattice parameters are obtained they are useful in finding the composition of the thin film. The smaller the lattice parameter the denser the thin film. To find the composition, the lattice parameter is compared to the known lattice parameters of the compounds likely to exist in the film. The reported value for uranium mononitride's lattice parameter is 0.498 nm and it is 0.547 nm for uranium dioxide [21,32-34]. The results from the TEM measurements state that the lattice parameter for the uranium nitride and uranium oxide samples studied is 0.489 nm and 0.549 nm respectively. These values give us crystal densities of 13.56 g/cm³ for the UN samples

and 10.96 g/cm^3 . These results agree well with our expectation that sample UN04 was indeed mostly uranium mononitride and that sample UO 18 was mostly uranium dioxide.

2.3 Reflectance Measurements at the ALS

Sample reflectances were measured at the Advanced Light Source (ALS) at Lawrence Berkley National Laboratory at the University of California-Berkley on beamline 6.3.2. This beamline has a reflectometer setup with three gratings (200 lines/mm, 600 lines/mm, and 1200 lines/mm) which allow the user to measure sample reflectance from 1 to 24.8 nm (50 to 1300 eV) at various angles [35]. Various filters coupled with order sorters and the gratings select the desired wavelength range as seen in Fig. 18.

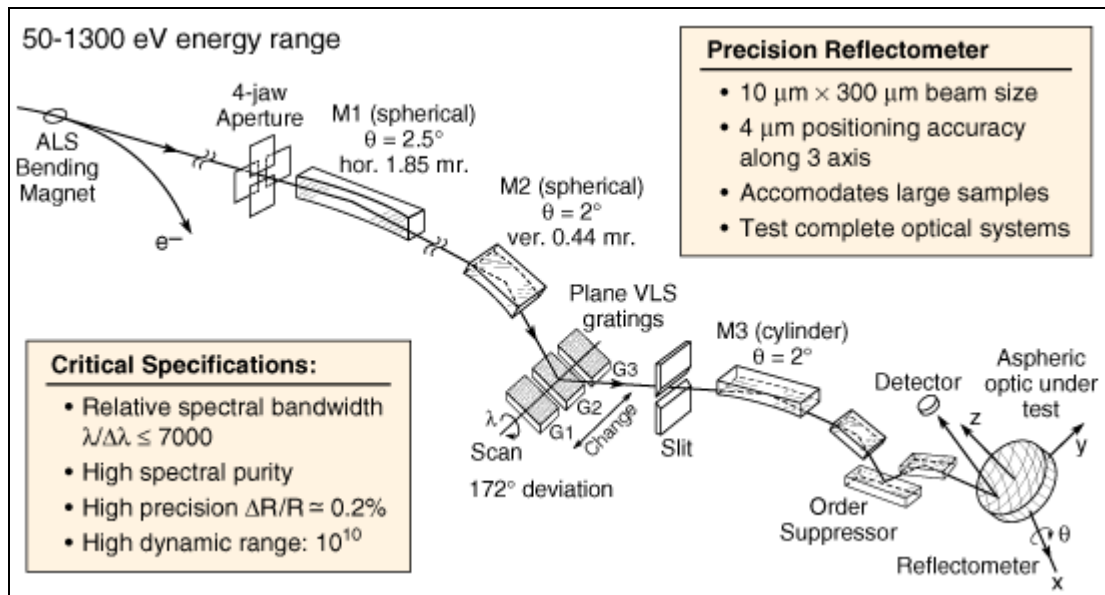


Fig. 18: Schematic of beamline 6.3.2 at the ALS [9,35].

Small discrepancies in the reflectances of different wavelength regions exist at the points where the filters must be used. These discrepancies may be due to imperfections

order suppression or due to small alignment problems either in the sample stage or with the filter, order suppressor system. These discrepancies can be seen in Fig. 19 at 4.5, 6.6, and 8.5 nm, and 8.5 nm.

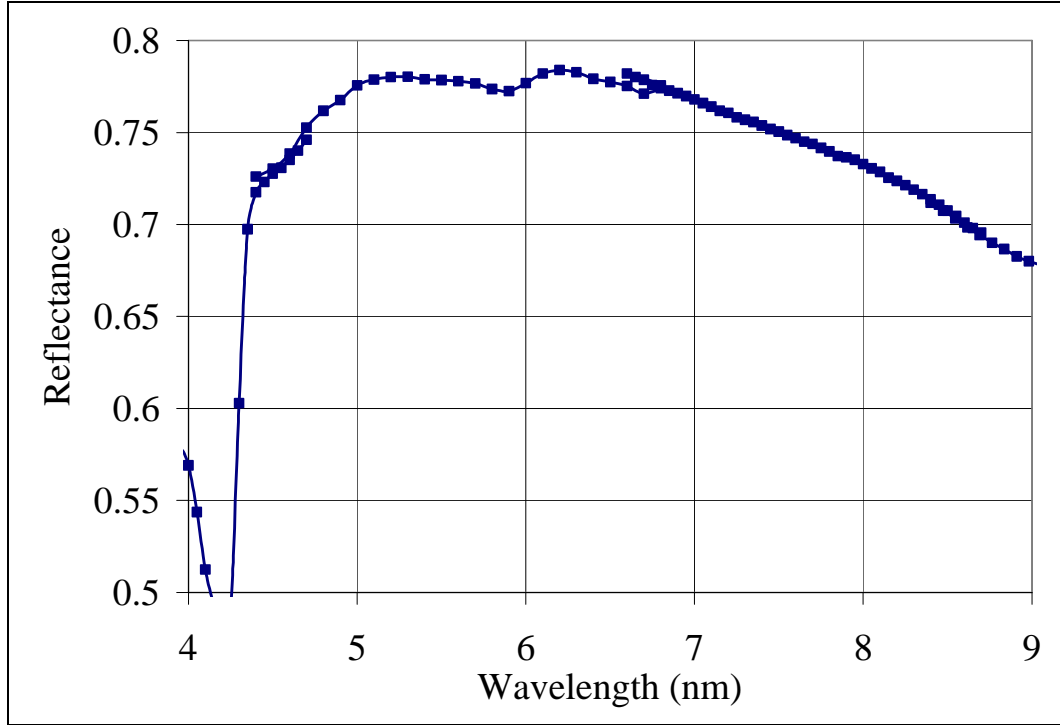


Fig. 19: Measured reflectance of UOx from ALS beamline 6.3.2at 5°. Notice the slight discrepancies at 4.5, 6.6, and 8.5 nm in the reflectance. Possible reasons for the small discrepancies could be imperfect order suppression or small alignment problems.

For each wavelength scan, and I_0 was taken by removing the sample and then taking data of only the source beam. Additionally, background noise scans were taken by completely blocking the source and collecting data. The process of normalization to extract reflectances is given by

$$R = \frac{I_r - I_d}{I_0 - I_d} \cdot \frac{B_0}{B_r} \quad (11)$$

where I_r is the photodiode current, I_0 is the photodiode current of normalization run (in beam path with no sample), I_d is the photodiode current of dark current offset, B_0 is the beam current at time of I_0 run, and B_r is the beam current at time of I_r run. This process is described in more detail along with further details on beamline 6.3.2 at the CXRO webpage and can be found in Underwood [35].

Chapter 3

Reflectance Comparison, Analysis, and Applications

3.1 Reflectance Comparison

Here I review the 2.5 to 12 nm portion of the reflectance data measured at ALS Beamline 6.3.2 on June 13-15, 2003, November 19-21, 2003, and February 12-15, 2004. I separate the data presented here into three figures depending upon the grazing incidence angle at 5°, 10°, and 15°. Each chart has five lines labeled respectively as UO₂, UN, NiO on Ni, Ir, and Au.

As shown in Fig. 12, at 5° uranium oxide and uranium nitride reflect more than nickel, gold, and iridium from 3.6 to 8.5 nm. At this lower grazing incidence angle, the uranium compounds have a maximum reflectance of about 80% from 5.2 to 6.6 nm as shown in Fig. 20. This value is 20-40% greater than the reflectance of nickel and even more than gold and iridium here.

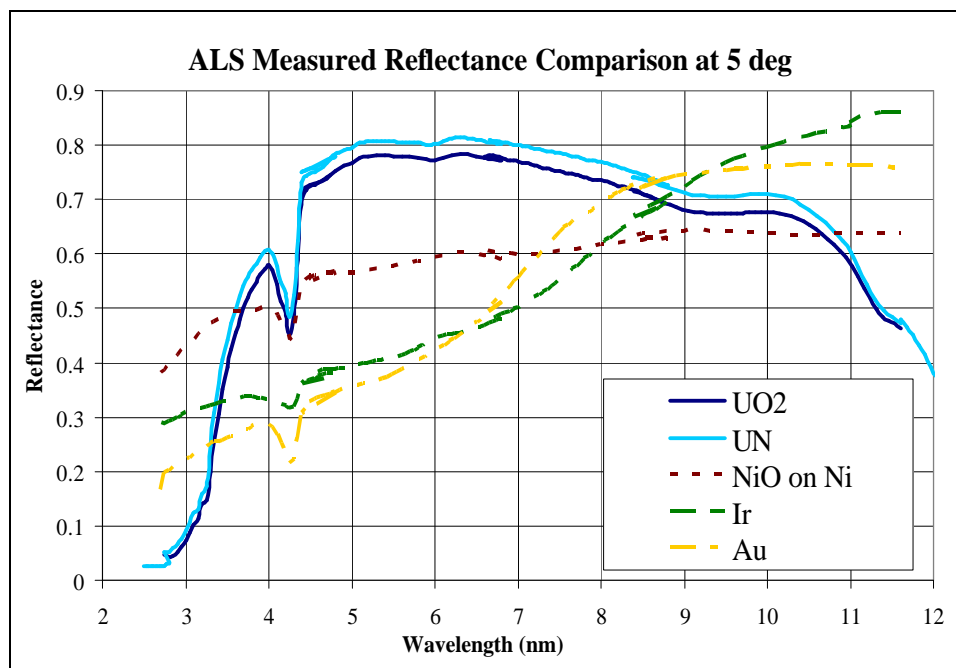


Fig. 20: Measured reflectance of UO₂, UN, NiO on Ni, Ir, and Au at 5° from 2.7 to 11.6 nm.

Notice the dip in reflectance of all three graphs at about 4.3 nm (285 eV). We previously suggested that this may correspond to the absorption edge of carbon near 284 eV indicating perhaps the presence of an adventitious thin organic layer [1-3]. However, x ray absorption near edge structure (XANES) data, which are presented below, indicates that uranium might have one or more absorption resonances here. In Fig. 20, we also should notice two interesting features of uranium oxide and uranium nitride. First, we notice a feature similar to an interference minimum at about 9.4 nm which we will see appear more strongly at higher angles. Second, we notice an apparent absorption dip at 11.4 nm.

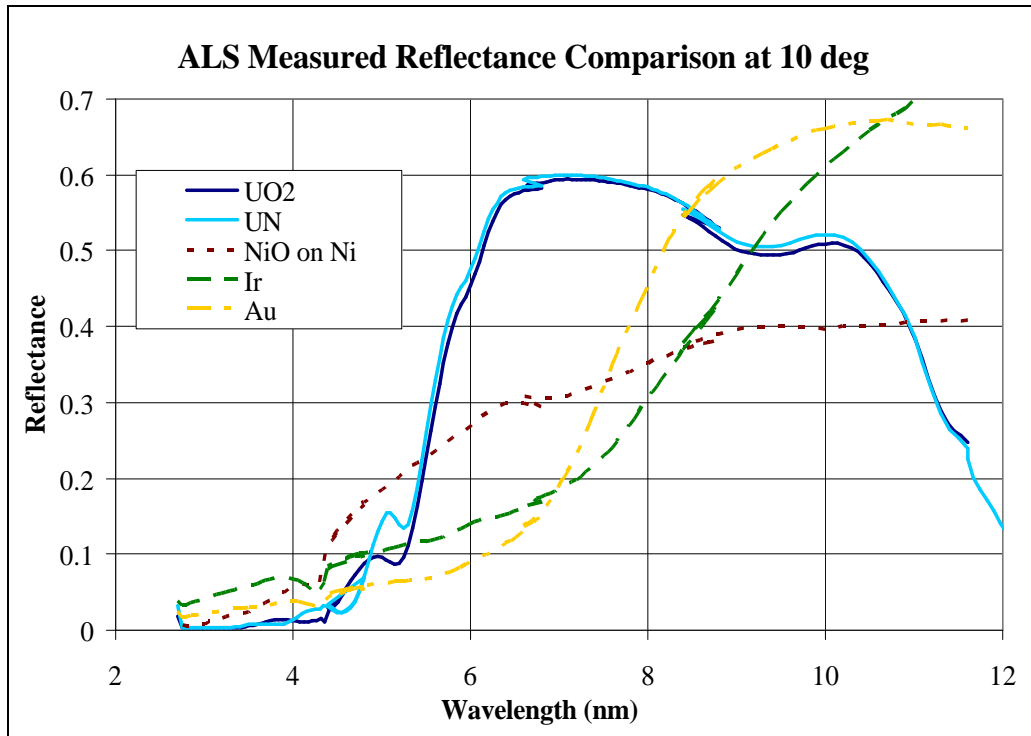


Fig. 21: Measured reflectance of UO₂, UN, NiO on Ni, Ir, and Au at 10° from 2.7 to 11.6 nm.

The next figure (Fig. 21) shows the reflectance comparisons of uranium to the standard coatings at 10° grazing incidence. First, notice that again an absorption edge appears near 4.3 nm. The reflectance of these uranium-compound samples exceeds that of nickel at 5.5 nm and continues at nearly double the reflectance of nickel over most of this range until at 10.5 nm it falls below the reflectance of our NiO on Ni film. By closer examination, discrepancies in the reflectance from one wavelength range to the other can be observed. Also, we notice in Fig. 21 that once again the absorption dip for the uranium-compounds at 11.4 nm is more gradual and does not rise again as quickly as calculated data shows (see Fig. 2 on page 4). Furthermore, we see more pronounced the presence of a minimum in uranium's reflectance at 10 nm.

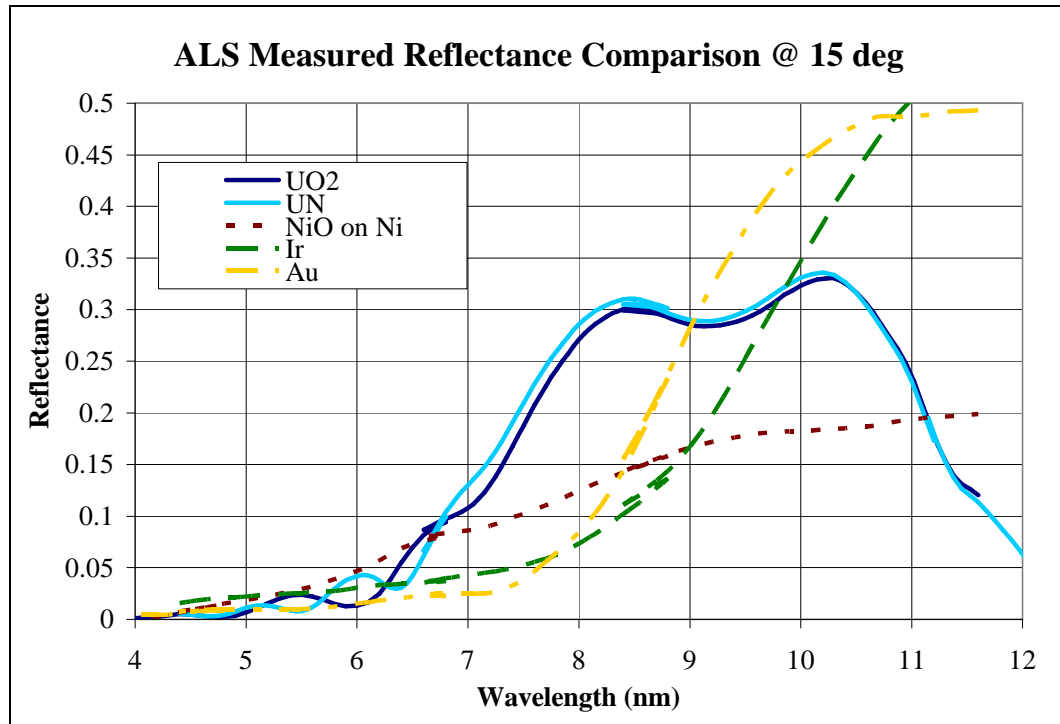


Fig. 22: Measured reflectance of UO₂, UN, NiO on Ni, Ir, and Au at 15° from 2.7 to 11.6 nm.

At 15°, uranium oxide reflects more than nickel, iridium, and gold at 6.3 nm and more than nickel at 10.9 nm. As seen in Fig. 22, the uranium samples reach a maximum reflectance of 33% at 10.3 nm.

3.2 Comparison to Calculated Reflectance

The reflectance curves for UN and UO₂ are nearly coincident. The reflectance of UN is greater than UO₂ in agreement with the reflectance of UN computed using the bulk density (14 g/cm³), but it is only slightly greater, whereas it should be ~10% larger. XPS examination of our UN films—not shown here but included in Urry [5] and Adamson [22]—indicates that their surface is UO₂. It may be necessary to deposit UN at high temperatures and/or by bias sputtering to realize bulk UN density and better stability.

As stated earlier, there is a feature apparent at 4.3 nm in the curves in Figs. 20-22. Since it is present in Au, Ir, and Ni as well as the uranium compounds it likely has a common origin, which we associate with carbon contamination. However, we notice that the feature is particularly pronounced in the uranium plots. In an effort to determine whether this feature can be attributed only to the presence of carbon, we modeled different structures of uranium oxide using the CXRO website as seen in Fig. 23 [9,36-40].

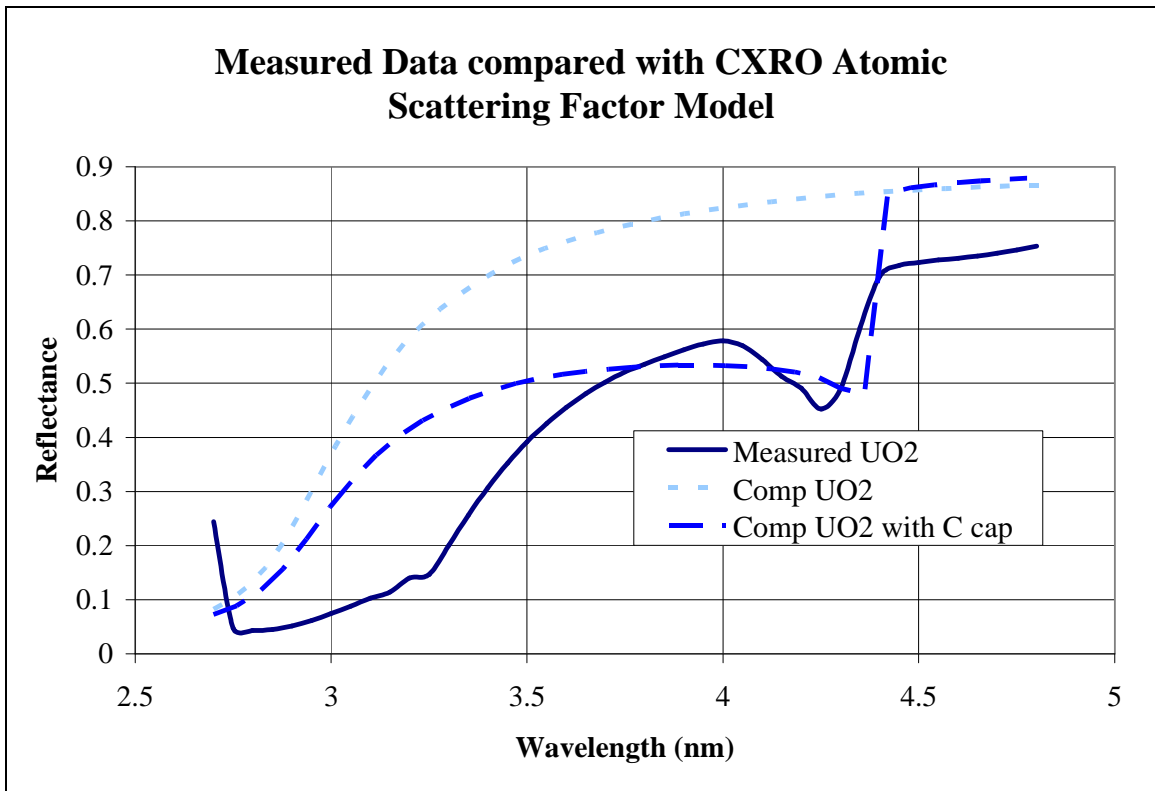


Fig. 23: Reflectance comparison of measured uranium oxide and calculated reflectance from different structures computed using the CXRO website [9,36-40]. Notice how the presence of carbon does not accurately match the absorption resonance at about 4.3 nm. Additionally the amount of carbon needed to achieve the appropriate depth of the feature is an unlikely 3 nm of carbon. An alternative explanation for the feature is the presence of an absorption resonance in uranium not reported by the CXRO website.

Fig. 23 shows a comparison of measured uranium oxide reflectance and reflectances from different structures calculated using the CXRO website [9,36-40]. Notice how the presence of carbon does not accurately match the absorption resonance at about 4.3 nm. Additionally the amount of carbon needed to achieve the appropriate depth of the feature is an unlikely to be 3 nm. An alternative explanation for the feature is the presence of an absorption resonance in uranium not reported by the CXRO website. This could be due to the fact that some of the references used bulk samples instead of thin films or that they used pure uranium samples to determine the optical properties of uranium. This fact increases the reason why thin-film uranium constants need to be reexamined in detail.

Several sources report x-ray emissions from uranium at 294.5 eV (4.21 nm) and 286.3 eV (4.33 nm) [21, 32-34]. Absorption features can occur near edges if the upper level is near the continuum. To ascertain whether any features in this energy range exists, a XANES (x-ray absorption near-edge structures) study of uranium oxide was performed at the ALS. XANES measures the electron current from a sample as a function of energy (or wavelength) of the incident light. As the energy is increased a point comes when photoelectrons can be emitted. Their loss from the sample is made up by current flowing from ground through a wire attached to the sample. The small current (typically less than 10^{-10} A) is measure by an electrometer.

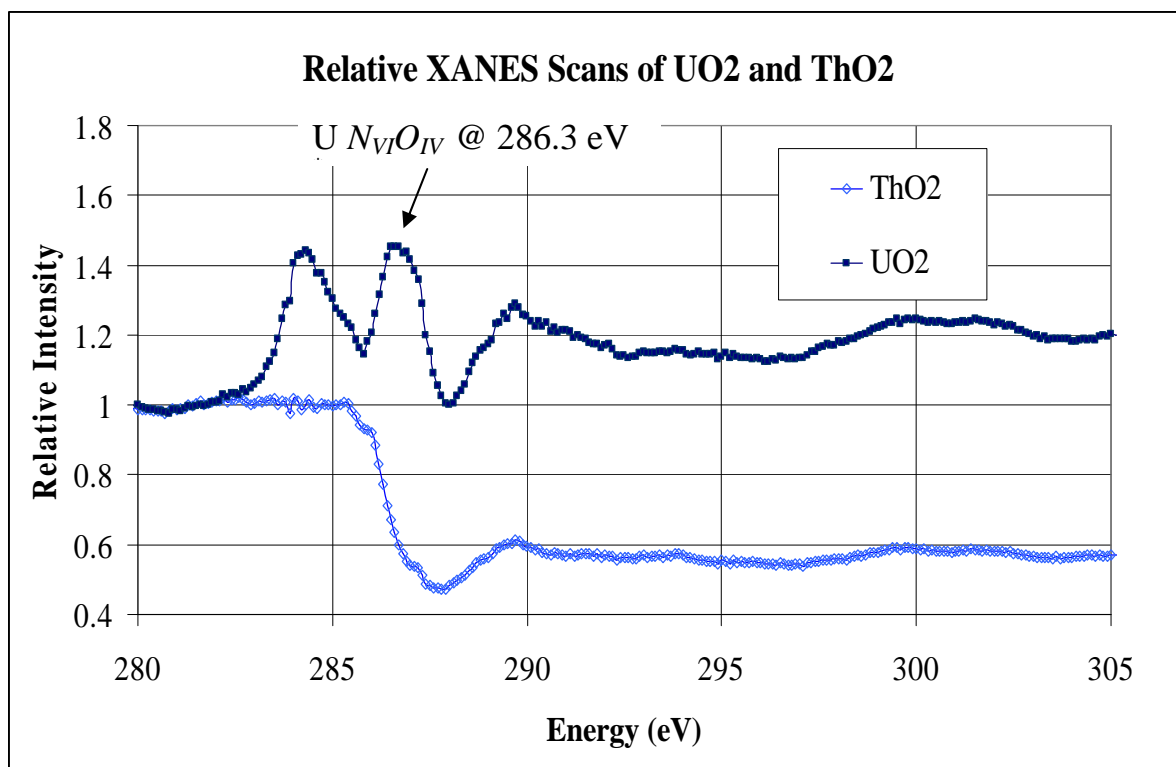


Fig. 24: X-ray absorption near edge structure (XANES) data taken at the ALS of uranium oxide and thorium oxide. The presence of an absorption resonance at 285 in uranium oxide and its absence in thorium oxide indicate that uranium does have an absorption resonance near 4.3 nm that is not reported in the existing optical properties at CXRO.

Fig. 24 shows the XANES data of thorium oxide and uranium oxide. The two have been normalized to carbon (we used a blank spot on the conducting carbon tape onto which the samples were attached) to minimize the effect which carbon contamination could have. As we can see, the presence of an absorption resonance can clearly be seen in uranium near 285 eV (4.3 nm) whilst no resonance appears in thorium at this energy. We regard this as evidence that the optical constants of uranium compounds need to be investigated further in this region of the spectrum.

3.3 Applications for Uranium Based Optics

As can be seen from the reflectance plots from section 3.1, the primary application for uranium compound thin films will be for EUV and soft x-ray reflectors. As stated earlier, these reflectors will have abundant applications in astronomy, medical and biological imaging, and other glancing incidence mirrors in the 2.7-11.6 nm range.

Another potential application for uranium in the EUV is as a notch filter. A notch filter is made of a system consisting of a thin film filter whose absorption edge matches the reflectance fall off of an associated mirror (see Attwood pages 78 and 79 for more discussion) [19]. These filters-mirror pairs are moderate pass filters which block the photons of energy above the mirror's reflectance fall off and below the filter's absorption edge. Uranium compounds might provide the mirror to such a notch filter at between 3-5 nm depending upon the incident angle (see Figs. 20-22) and perhaps at the other reflectance fall off at 15 nm. Uranium compounds might provide the filter portion of a notch filter at its strong absorption edge at 12 nm.

Perhaps the most exciting potential application for uranium compounds in the EUV is as a Fresnel zone plate lens. A zone plate is a microscopic plate (radii are on the order of between 100 nm and 100 microns depending on the photon energy of interest) consisting of concentric rings of thin material that are thinner as the radius of the ring increases. There is a corresponding amount of empty space between each ring so that each ring and vacant space has the same area. These zone plates work as diffractive lenses and are crucial in many types of EUV or soft x-ray imaging systems such as EUV

microscopes for biological, medical, and materials science imaging. Attwood describes in depth the theory of zone plate lenses for the EUV (see Chapter 9) [19].

Theory predicts that for a zone plate with perfectly absorptive rings, the efficiency of each order (i.e. the ratio of the intensity of light focused into the m^{th} focal point compared to the intensity of light incident upon the lens) is given by

$$\mathbf{h}_m = \begin{cases} 0.25 & m = 0 \\ \frac{1}{m^2 p^2} & m = \text{odd} \\ 0 & m = \text{even} \end{cases} \quad (12)$$

where m is the order diffractive focusing order. As we can see, the zeroth order receives 25% of the light (or in other words, 25% of the light passes straight through), the odd orders receive $1/m^2 p^2$ percent of the light, with about 10% focusing into the first order. 50% of the light is absorbed by the zone plate. However, for zone plates made of materials that are partially transparent, this order efficiency can greatly increase as described by Attwood [19] and Kirz [41]. Due to uranium's low beta, it is less absorptive in this region than many substances. Kirz shows that the diffractive order m efficiency of transmissive zone plates is given by

$$\mathbf{h}_m = \frac{1 + \exp\left(-2 \frac{\mathbf{b}\mathbf{f}}{d}\right) - \cos(\mathbf{f}) \exp\left(-\frac{\mathbf{b}\mathbf{f}}{d}\right)}{m^2 p^2} \quad (13)$$

where m is the diffractive order, d and β are the materials optical constants, and \mathbf{f} is given by

$$\mathbf{f} = 2p \frac{td}{l} \quad (14)$$

with zone plate thickness t and wavelength λ . The efficiency of our uranium samples can be computed at the values for d and β given by Lunt for UO_2 and for the unknown

uranium oxidation state of her sample's top layer (probably a combination of UO_2 and UO_3) [4]. The efficiencies of 100 nm zone plates were computed using equations 3.2 and 3.3 and the constants from the CXRO website for gold, nickel, and germanium and are found in Table 3 [9-13]. The wavelengths and efficiencies are highlighted where uranium has a higher first order efficiency than gold, nickel, and germanium.

Energy (eV)	Au	Ni	Ge	UO_2	UO Top
99.2	0.1013	0.1013	0.1013	0.0971	0.0925
124	0.0970	0.1013	0.1014	0.1013	0.1015
145.9	0.1098	0.1013	0.1020	0.1000	0.0989
182.4	0.1219	0.0998	0.1049	0.1781	0.1771
221	0.1112	0.0985	0.1117	0.2857	0.2623
270	0.1013	0.1311	0.1160	0.1811	0.1710

Table 3: First order efficiency for 100 nm thick zone plates of various materials

As can be seen from Table 3, the efficiencies of uranium at 182.4, 221, and 270 eV are much higher than the efficiencies of other commonly used materials. At 221 eV (5.6 nm), uranium more than doubles the efficiency of the other materials.

Chapter 4

Conclusion

Uranium containing thin-film reflectors are more reflective than traditional thin film coatings (nickel, iridium, and gold) over a large range of angles and wavelengths as predicted by their tabulated optical constants. Specifically, uranium oxide and uranium nitride reflect more than standard coatings at 5° grazing incidence from 4.5 to 8.5 nm, at 10° from 5.5 to 9 nm, and at 15° grazing incidence from 6.5 to 9 nm. Uranium-based coatings have been used successfully in the past and hold great promise for further applications in EUV/soft x-ray optics. We therefore recommend that uranium oxide-based mirror coatings should be developed and implemented for future projects where broadband, low angle, soft x-ray mirrors are required. Another finding of this report is that the complex indices of refraction probably differ noticeably from the reported values. Evidence is shown that an absorption resonance exists in uranium at 4.3 nm (283 eV).

Additionally, we see that reflectances given by uranium's previously reported optical properties do not generate the shallow reflectance minimum at about 9.5 nm in the uranium reflectance measurements nor that the absorption edge is not at approximately 11.1 nm as reported. We are in the processes of determining the index of refraction for naturally oxidized uranium and uranium nitride over the soft x-ray and EUV range in conjunction with the Center for X-ray Optics. Uranium has many advantages to other commonly used materials (gold, nickel, iridium, etc.) for EUV optics such as higher reflectance from 2.7 to 11.6 nm for thin film mirrors and greater calculated efficiencies at 4.6, 5.6, and 6.8 nm for Fresnel zone plates.

REFERENCES

1. R. L. Sandberg, D. D. Allred, J. E. Johnson, R. S. Turley, "A comparison of uranium oxide and nickel as single-layer reflectors from 2.7 to 11.6 nm," in *Advances in Mirror Technology for X-Ray, EUV Lithography, Laser, and Other Applications*, edited by Ali M. Khounsary, Udo Dinger, Kazuya Ota, Proceedings of SPIE Vol. 5193 (SPIE, Bellingham, WA, 2004) 191-203.
2. R. L. Sandberg, D. D. Allred, L.J. Bissell, J.E. Johnson, R.S. Turley, "Uranium Oxide as a Highly Reflective Coating from 100-400 eV," in *SYNCHROTRON RADIATION INSTRUMENTATION: Eighth International Conference on Synchrotron Radiation Instrumentation*, San Francisco, A.I.P., pp. 796-799, 2004.
3. R.L. Sandberg et al., in *AIP Conf. Proc. of International Conference on Metallurgical Coatings And Thin Films*, 2004 (In the press).
4. S. Lunt, "Determining the Indices of Refraction of Reactively Sputtered Uranium Dioxide Thin Films from 46 to 584 Angstroms," (Masters Thesis) Dept. of Physics and Astronomy, Brigham Young University, 2002.
5. M. K. Urry, "Determining Optical Constants of Uranium Nitride Thin Films in the Extreme Ultraviolet (1.6-35 nm)," (Senior Thesis) Dept. of Physics and Astronomy, Brigham Young University, 2004.
6. D.D. Allred, R. S. Turley, and M. B. Squires, "Dual-function EUV multilayer mirrors for the IMAGE mission," in *EUV, X-Ray and Neutron Optics*, Carolyn A. Macdonald, Kenneth A. Goldberg, Juan R. Maldonado, H. Heather Chen-Mayer, and Stephen P. Vernon, Editors, Proceedings of SPIE 3767, pp.280-287, SPIE, Bellingham, WA, 1999.

7. David D. Allred, Matthew B. Squires, R. Steven Turley, Webster Cash, and Ann Shipley, "Highly Reflective Uranium Mirrors for Astrophysics Applications," in X-ray Mirrors, Crystals and Multilayers, Andreas K. Freund, Albert T. Macrander, Tetsuya Ishikawa, and James. T. Wood, Editors, Proc. SPIE 4782, pp. 212-223, SPIE, Bellingham, WA, 2002.
8. D. Oliphant, "Characterization of Uranium, Uranium Oxide and Silicon Multilayer Films," (Masters Thesis) Dept. of Physics and Astronomy, Brigham Young University 2000.
9. http://www-cxro.lbl.gov/optical_constants/, accessed July, 2003, or contact Eric Gullikson from the webpage for additional questions.
10. B.L. Henke, E.M. Gullikson, and J.C. Davis. "X-ray interactions: photoabsorption, scattering, transmission, and reflection at E=50-30000 eV, Z=1-92," Atomic Data and Nuclear Data Tables, Vol. **54** (no.2), 181-342 (July 1993).
11. R. Soufli and E. M. Gullikson, "Reflectance measurements on clean surfaces for the determination of optical constants of materials in the EUV/soft x-ray region," Applied Optics **36**, 5499-5507 (1997).
12. C. S. Nelson, et al., "Efficiency measurements and modeling of the Advanced X-ray Astrophysics Facility (AXAF) high-energy transmission gratings," Proceedings of the SPIE Vol. 2280, 191-203 (July 1994).

13. E. M. Gullikson et al., "Absolute photoabsorption measurements of Mg, Al, and Si in the soft-X-ray region below the L_{2,3} edges," *Physical Review B* 49, 16283-8 (15 June 1994).
14. Hans Pew, formally of MOXTEK, Inc., Private Communication.
15. Webster Cash, University of Colorado, Personal Communication
16. E.H.P. Cordfunke, The Chemistry of Uranium, Elsevier Publishing Co, Amsterdam, 1969.
17. L. Black, F. Miserque, T. Gouder, L. Havela, J. Rebizant, and F. Watsin, *Journal of Alloys and Compounds*, 315, (2001) 36-41
18. K. Takemoto, et. al., *AIP Conf. Proc.* 507 (2000) 446
19. D. Attwood, *Soft X-rays and Extreme Ultraviolet Radiation* (Cambridge University Press, Cambridge, 1999).
20. Private Communication, Ritva Keski-Kuha, Goddard Space Center
21. D. R. Lide (ed.), CRC Handbook of Chemistry and Physics, Section 10, 71st edn. CRC Press, Boca Raton, 1990-91, 256
22. K.R. Adamson, "Determining Chemical Composition through X-Ray Photoelectron Spectroscopy", (Senior Thesis) Dept. of Physics and Astronomy, Brigham Young University, 2004
23. H. Drury and M. Rowberry, May 2003 International Science Fair, Columbus OH, USA.
24. Program for EUV and X-ray reflectance calculations, courtesy of Prof. David L. Windt: windt@astro.columbia.edu. <http://cletus.phys.columbia.edu/windt/idl>.

IMD's data files are the same as the CXRO's web site (see references [9-13] and for the specific primary sources from [10] Henke et al., see references [36-40]).

25. Y. A. Teterin, V. M. Kulakov, A. S. Baev, N.B. Nevzorov, I.V. Melnikov, V. A. Streltsov, L. G. Mashirov, D. N. Suglabov, A. G. Zelenkov. "A Study of Synthetic and Natural Uranium Oxides by X-Ray Photoelectron Spectroscopy." *J. Phys. Chem. Minerals.* **7**, 151-158 (1981).
26. R.E. Robinson, "Removing Surface Contaminants from Silicon Wafers to Facilitate EUV Optical Characterization", (Senior Thesis) Dept. of Physics and Astronomy, Brigham Young University, 2003.
27. R.E. Robinson, *et al.*, "Removing Surface Contaminants from Silicon Wafers to Facilitate EUV Optical Characterization," (To be published in *Journal of Vacuum Science and Technology*).
28. <http://www.weizmann.ac.il/surflab/peter/afmworks/>, November 4, 2003.
29. N. Farnsworth. "Roughness and other fun stuff." XUV Group Powerpoint Presentation (Brigham Young University, Provo, UT, 2004).
30. P. Debye. *Über die Intensitätsverteilung in den mit Röntgenstrahl erzeugten Interferenzbildern.* *Verh. D. Deutsch. Phys. Ges.* **15**: 738.
31. P. Croce and L. Nevot. *Etude des couches minces et des surfaces par réflexion rasante, spéculaire ou diffuse, de rayons X.R.* *De Physique Appliquée* **11** (1976): 113-125.
32. Flügge and Martensson, *J. Elect. Spect.*, **21**, 275, (1980).
33. Cardona, M. and Ley, L., *Photoemission from Solids*, Springer, Verlag, Heidelberg, (1978).

34. Bearden, J. A. and Burr, A. F., *Rev. Mod. Phys.*, 39, 125 (1967).
35. J.H. Underwood *et al.* "Calibration and standards beamline 6.3.2 at the Advanced Light Source." *Rev. Sci. Instrum.*, 67 (9), 1-5 (1996).
36. N. K. Del Grande, J. H. Mallet, and A. J. Oliver, (Unpublished data and also data listed in Lawrence Livermore National Laboratory, CA, UCRL-50174, 1969).
37. N. K. Del Grande and A. J. Oliver, *Bull. Am. Phys. Soc.* 18, 2230-2237 (1973).
38. M. Cukier, P. Dhez, F. Wuillieumier, and P. Jaegle, *Phys. Lett. A* 48, 307-308 (1974).
39. N. K. Del Grande, and A. J. Oliver, Lawrence Livermore National Laboratory, Livermore, CA, UCRL-85683 (1981).
40. N. K. Del Grande, *Proc. SPIE* 691, 2-10 (1986).
41. J. Kirz, *JOSA* 64, 301 (1974).